A CPT-BASED ^{87}Rb ATOMIC CLOCK EMPLOYING A SMALL SPHERICAL GLASS VAPOR CELL

Ido Ben-Aroya, Matan Kahanov, and Gadi Eisenstein
Department of Electrical Engineering, Technion, Haifa 32000, Israel
E-mail: *bido@tx.technion.ac.il*

Abstract

This paper describes the performance of an atomic clock based on Coherent Population Trapping in a ^{87}Rb vapor. The clock employs a small spherical glass cell and exhibits a performance which is comparable to that of a commercial atomic clock. A resonance width of less than 200 Hz leads to short term stability of $3\times10^{-11}/\sqrt{\tau}$ for time constants of 0.5 sec to 200 sec. The relative frequency stability is better than 10^{-10} with a slow drift of only 0.1 mHz per day.

I. INTRODUCTION

Miniature atomic clocks with dimensions of the order of 1 cm^3 and with a power consumption of only few tens of mW have been researched extensively in the past few years **[1]**. These small frequency standards, termed chip scale atomic clocks (CSACs) have an expected performance, in terms of Allan deviation, of $\sigma_y(\tau=1\ \text{day})<1\times10^{-11}$. Implementation of a CSAC requires construction of a tiny atomic vapor cell, usually by means of MEMS technology. The physical process employed in most of the CSACs is Coherent Population Trapping (CPT) **[2, 3, 4]** with which there is no fundamental limitation to size reduction.

CPT uses two coherent radiation fields which couple two non-degenerate hyperfine split levels to the same exited state (Λ-System). Those coherent fields are detuned relative to each other by the hyperfine splitting frequency of the ground level and are phase-matched. A convenient source for these radiation fields are the two first side bands of single mode Vertical Cavity Surface Emitting Laser diode (VCSEL), which is directly modulated at half the ground state hyperfine splitting frequency. Two, naturally coherent, side bands, which are detuned by the hyperfine splitting frequency, are created and serve to excite the dark resonance **[5]**. The advantage of VCSELs lies in their small size, low power consumption, and wide modulation bandwidth **[5]**. Moreover, high quality VCSELs are available at a variety of wavelengths enabling CPT resonance in both cesium **[6,7]** and rubidium atoms **[8]**.

The small size of the vapor cell in a CSAC together with various noise sources and instabilities stemming from the VCSEL require complex stabilization procedures in order to achieve an acceptable performance of the small clocks **[9,10]**. Significant progress has been reported in that respect using two somewhat different constructions **[11,12]**. Another approach, which employs an optoelectronic oscillator containing a small ^{87}Rb cell as an optical domain filter, has also been demonstrated recently **[13]**, but its performance is still inferior to that of conventional CPT clock configurations such as **[14]**.

This paper reports on a CPT-based atomic clock which uses a small spherical glass cell, thereby avoiding

the need for MEMS technology. The cell which is constructed using standard glassblowing techniques is a few millimeters in diameter and is similar to the one used recently for magnetic sensing **[15]**. The CPT resonance is excited within an ^{87}Rb vapor at the D_2 line, which requires a VCSEL emitting at 780.24 nm. The Zeeman degeneracy is removed by a controlled magnetic field and, therefore, the clock transition involves the hyperfine-split levels F = 1, m_f = 0 and F = 2, m_f = 0 (0-0 transition). The locked system employs a 10 MHz Oven Controlled Voltage Controlled Crystal Oscillator (OCXO), which serves as the reference to a microwave synthesizer operating at half the hyperfine frequency – 3417.3 MHz. The system outputs a stabilized 10 MHz signal.

The results we describe are for a laboratory (not miniaturized) system. A typical CPT resonance fits to a Lorentzian functional shape with a width of less than 190 Hz and a contrast of about 0.5%. The change in absorption due to the CPT resonance is detected by the sensitive FM spectroscopy method, which maps out the absorption and refraction spectra **[16]**. The refraction spectrum exhibits a particularly sharp slope, which allows for easy and reliable locking of the clock.

The clock performance we obtain approaches that of commercial ^{87}Rb clocks **[17]** (which do not use CPT) and resembles results obtained in CPT-based ^{133}Cs clocks which employ a large cylindrical cell **[6**]. The short-term stability is typically $\sigma_y=3\times10^{-11}/\sqrt{\tau}$ for time constants of 0.5 sec to 200 sec. This result is one and a half orders of magnitude worse than the shot noise limit of $7\times10^{-13}/\sqrt{\tau}$, which was calculated from the characteristics of the CPT resonance **[3]**. The difference is attributed to noise sources originating from the VCSEL and to environmental instabilities, some of which will be corrected when the system will be miniaturized. The long-term frequency stability of the system was measured by sampling the 10 MHz output every few seconds over a period of more than 24 hours. The frequency deviation is of the order of 0.5 mHz (5×10^{-11}) with an accompanying slight drift of 0.1 mHz per day (10^{-11} / day).

II. EXPERIMENTAL SETUP

The CPT clock is described schematically in Figure 1. A temperature-stabilized single-mode VCSEL emitting around 780.24 nm (which matches the D_2 transition in ^{87}Rb) is driven by a low-noise DC current source coupled to a microwave signal at a frequency equal to half the ^{87}Rb hyperfine splitting frequency – 3417.3 MHz. The first two modulation side bands serve as the two coherent electromagnetic fields required for CPT. The VCSEL output is collimated and its polarization is set to be circular. The light impinges a ball-shaped glass vapor cell with an internal diameter of about 5 mm and an external diameter of 6 mm. The vapor cell, a photograph of which is shown in the insert of Figure 1, contains a mixture of pure ^{87}Rb atoms and a buffer gas. The cell, together with a controlled heater and a large solenoid, are placed in the middle of a three-layer μ-metal box which attenuates the environmental magnetic field. The cell temperature is stabilized around the optimum temperature of 66ºC to a level of 1 mK. A homogeneous magnetic field of 35 μT pointing in a direction parallel to the optical axis is generated around the vapor cell by the solenoid in order to lift the Zeeman degeneracy thereby isolating the 0-0 (clock) transition. The transmitted light through the cell is detected by a large area (1 cm^2) silicon detector.

The surrounding electronics contains two control loops: the diode wavelength stabilization servo loop and a Frequency-Locked Loop (FLL) or the clock loop. The wavelength stabilization loop uses changes in the VCSEL bias to compensate for variations in the emitted wavelength. The wavelength is stabilized around the minimum transmission peak. Due to various noisy features of the physical process, it is necessary to detune the locking point relative to the peak **[18**]. In the present system, we used a red shift of approximately 60 MHz.

The clock loop is stabilized on the zero crossing point of the steep slope of the FM spectroscopy output signal mostly related to the refraction spectrum. The FM modulation frequency was set to be approximately four times the CPT resonance width and the modulation index was set to be 0.5 in order to maximize the measured CPT resonance slope. The detected signal is analyzed by a lock-in amplifier whose reference is the FM modulating signal. The lock-in amplifier outputs comprise different odd derivatives of the absorption profile of the medium **[16]**. In the locked state, the system error signal, which is generated at the lock-in amplifier, is first integrated and then fed to a 10 MHz OCXO which serves, in turn, as the reference for the microwave synthesizer.

The stabilized 10MHz output signal is sampled by a Pendulum CNT-90 counter and a Timing Solutions 5120A phase noise test set for analysis. Both are referenced by an Accubeat model AR-60 Rb atomic clock.

III. EXPERIMENTAL RESULTS

The experimental results are described in two separate parts. The first details the characteristics of the dark resonance, while the second presents the performance of the atomic clock. The first part, dealing with open-loop measurements, includes: basic absorption features, CPT resonance measurements, and several dependencies of resonance central frequency on controlled environmental parameters. The second subsection, on closed-loop measurements, describes the short- and long-term performance of the atomic clock.

IIIA. OPEN-LOOP MEASUREMENTS

The first characterization of the vapor cell included a detailed investigation of its absorption profile. The absorption is examined by scanning the emitted wavelength, which is controlled by the diode DC bias. The VCSEL wavelength scan is accompanied, of course, by a change in intensity which is, however, easily compensated for in the measured absorption spectrum **[19]**. Figure 2a presents a typical two-peak absorption profile measured with the spherical cell operating at a temperature of 75ºC. This test is essential for the verification that a sufficient quantity of ^{87}Rb atoms exists inside the small cell after it is sealed. A second absorption spectrum obtained by scanning the bias in the presence of a constant-amplitude, constant-frequency (3.4173 GHz) microwave drive signal is shown in Figure 2b. The complex multi-peak spectrum results from the VCSEL nonlinearity, which generates harmonics. The comb of VCSEL spectral lines scans the multi-line absorption spectrum of ^{87}Rb, yielding the complex result of Figure 2b **[19]**.

Since the modulation frequency is half the hyperfine splitting frequency, a local minimum is obtained every 3.4173 GHz. Each dip is the result of a different pair of side bands coinciding (spectrally) with the ^{87}Rb absorption peaks. The largest peak, marked by a red arrow, is attributed to the first two side bands of the modulated VCSEL – the (+1;-1) peak. This peak is exclusively used to excite the CPT process in the present experiments. Since the modulation response of the diode is sensitive to its operational temperature, the RF power was set to achieve maximum absorption in the (+1;-1) peak. At 20ºC, the optimum RF power is +1.5 dBm.

A typical measured CPT resonance is presented in Figure 3. The resonance, which was obtained by a direct transmission measurement, fits a Lorentzian with a width of 186 Hz. The CPT contrast, defined as the ratio of the peak detected signal and the background signal **[3]**, was measured to be 0.5%. The width

and its contrast determine the shot-noise limited stability of a clock to be locked on this resonance. For the resonance shown in Figure 3, the value is approximately $7\times10^{-13}/\sqrt{\tau}$.
Figure 4 describes a measurement of the same resonance by the FM spectroscopy technique. The red curve (the y output of the lock-in amplifier) is mainly attributed to the first derivative of the absorption, while the blue curve (x output) is related to the second derivative of the dispersion. The slope of the x output is extremely steep and is, therefore, suited well for locking the clock.

The influences of controlled environmental parameters on the resonance frequency are described in Figures 5 and 6. Since the system exhibits but a moderate signal-to-noise ratio, we employed the FM spectroscopy method to enhance the measured signal, with its zero crossing point being the resonance frequency. Figure 5a shows the measured resonance frequency dependence on the cell operational temperature. The linear change is caused by an imperfect balance of the buffer gas and will be corrected in future cells. Figure 5b shows the variation of the resonance frequency with magnetic field. The changes are due to the second-order Zeeman effect and fit well to the predicted shifts of the 0-0 transition.

Optimization of the CPT resonance quality is described in Figure 6. Figures 6a shows the q factor (defined as the ratio of the resonance contrast to its width) **[3]**, while Figure 6b describes the steepness of the y output (represented by the red line in Figure 4), both as a function of cell temperature. We note that both parameters exhibit an optimum at the same temperature – 66 ^{o}C.

IIIB. CLOSED-LOOP MEASUREMENTS

The entire system shown in Figure 1 was tested for its short- and long-term frequency stabilities. The frequency of the stabilized 10 MHz output was sampled every few seconds during a period of more than 27 hours. The results are shown in Figure 7. The relative frequency drift lies within a range smaller than 1 mHz/10 MHz or less than 10^{-10}. We also note a very slight drift of about 0.1 mHz during those 27 hours or a relative drift of less than 10^{-11} / day.

The short-term stability (Allan deviation) of the output signal was measured at time constants ranging from 0.5 sec to 1000 sec. The results are shown in Figure 8. For time constants of 0.5 sec to 200 sec, the curve varies linearly with $\sqrt{\tau}$, attaining a value of 3×10^{-11} at 1 sec. The minimum observed Allan deviation value is 2.5×10^{-12} at 200 sec, beyond which it stabilizes and then starts to increase. Also shown in Figure 8 is a predicted Allan deviation curve which is based on a measurement of the noise accompanying the output of the lock-in amplifier (y output in Figure 4). The noise was measured by disconnecting the feedback loop at the lock-in amplifier output and measuring the variations of the error signal using the lock-in amplifier internal noise measurement function. The measurement is performed under conditions where the CPT remains properly tuned.

The predicted short term stability is $2\times10^{-11}/\sqrt{\tau}$, which is one and a half orders of magnitude larger than the shot-noise-limited performance predicted by the characteristics of the CPT resonance. The additional noise stems from several sources. A major issue is VCSEL wavelength and polarization **[20]** instabilities as well as amplitude noise (RIN) **[20]** to frequency noise transfer **[21,18]** due to the dispersive nature of the resonance. Moreover, the RF modulation index, temperature, power, and wavelength are strongly coupled in a VCSEL **[9,10]** so that noise and instabilities in any operational condition are easily enhanced.

Other noise sources originate from the electronics servo loops as well as the temperature-control mechanism and the magnetic field source. Above and beyond that, the temperature stability of the present large laboratory system is difficult to control, causing a deterioration of the stability at very long time

constants.

Finally, we note that the predicted curve in Figure 8 is lower than the measured curve. This difference is attributed to some uncertainty in the measurement of the Allan deviation as well as to inaccuracies in the noise measurements on which the prediction is based.

IV. CONCLUSIONS

In conclusion, we have presented a CPT based ^{87}Rb atomic clock which uses a small glass vapor cell. The system exhibits a narrow resonance width of less than 200 Hz with a contrast of ~0.5%. The clock performance resembles that of commercial (non-CPT) ^{87}Rb clocks and experimental atomic clock based on dark resonance in a large cylindrical vapor cell containing ^{133}Cs atoms. It exhibits a short-term stability of $3\times10^{-11}/\sqrt{\tau}$ for time constants of 0.5 sec to 200 sec. The relative frequency stability is better than 10^{-11} with a slow drift of only 0.1 mHz per day.

The Allan deviation at a time constant of 1 sec is larger by a factor of ~ 40 than the shot-noise limit expected from the characteristics of the CPT resonance. This deterioration is mainly due to noise mechanisms stemming from the VCSEL including wavelength, polarization, and amplitude instabilities. Some noise is also added by the electronic control circuitry. The long-term frequency instabilities are attributed mainly to environmental conditions, in particular temperature variations, which are difficult to control in the present (large) laboratory system.

V. ACKNOWLEDGMENT

This work was performance within the framework of developing a miniature atomic clock. The authors thank A. Stern and B. Levi of AccuBeat Ltd. and M. Rosenbluh of Bar Ilan University.

VI. REFERENCES

[1] R. Lutwak, P. Vlitas, M. Varghese, M. Mescher, D. K. Serkland, and G. M. Peake, 2005, *"The MAC – a Miniature Atomic Clock"* in Proceedings of 2005 Joint IEEE International Frequency Control (UFFC) Symposium and the 37th Annual Precise Time and Time Interval (PTTI) Systems and Applications Meeting, 29-31 August 2005, Vancouver, Canada (IEEE 05CH37664C), pp. 752-757.

[2] E. Arimondo, 1996, *"Coherent population trapping in laser spectroscopy,"* **Progress in Optics, 35,** 257-354.

[3] J. Vanier, 2005, *"Atomic clocks based on coherent population trapping: a review,"* **Applied Physics B, 81,** 421-442.

[4] N. Cyr, M. Têtu, and M. Breton, 1993, *"All-optical microwave frequency standard: a proposal,"* **IEEE Transactions on Instrumentation and Measurement, IM-42,** 640-649.

[5] C. Affolderbach, A. Nagel, S. Knappe, C. Jung, D. Wiedenmann, and R. Wynands, 2000, *"Nonlinear spectroscopy with a vertical-cavity surface-emitting laser (VCSEL),"* **Applied Physics B,** 407-413.

[6] J. Kitching, S. Knappe, N. Vukičević, L. Hollberg, and W. Weidmann, 2000, *"A microwave frequency reference based on VCSEL-driven dark line resonance in Cs vapor,"* **IEEE Transactions on Instrumentation and Measurement, IM-49,** 1313-1317.

[7] R. Lutwak, D. Emmons, W. Riley, and R. M. Garvey, 2003, *"The chip-scale atomic clock-coherent population trapping vs. conventional interrogation,"* in Proceedings of the 34th Annual Precise Time and Time Interval (PTTI) Systems and Applications Meeting, 3-5 December 2002, Reston, Virginia, USA (U.S. Naval Observatory, Washington, D.C.), pp. 539-550.

[8] S. Knappe, P.D.D. Schwindt, V. Shah, L. Hollberg, and J. Kitching, 2005, *"A chip-scale atomic clock based on ^{87}Rb with improved frequency stability,"* **Optics Express, 13,** 1249-1253.

[9] V. Gerginov, S. Knappe, V. Shah, P. D. D. Schwindt, L. Hollberg, and J. Kitching, 2006, *"Long-term frequency instability of atomic frequency references based on coherent population trapping and microfabricated vapor cells,"* **Journal of the Optical Society of America B, 23,** 593-597.

[10] V. Gerginov, V. Shah, S. Knappe, L. Hollberg, and J. Kitching, 2006, *"Atomic-based stabilization for laser-pumped atomic clocks,"* **Optical Letters, 31,** 1851-1853.

[11] S. Knappe, V. Shah, P. D. D. Schwindt, L. Hollberg, J. Kitching, L. Liew, and J. Moreland, 2004, *"A microfabricated atomic clock,"* **Applied Physics Letters, 85,** 1460-1462.

[12] R. Lutwak, J. Deng, W. Riley, M. Varghese, J. Leblanc, G. Tepolt, M. Mescher, D. K. Serkland, K. M. Geib, and G. M. Peake, 2005, *"The chip-scale atomic clock-low-power physics package,"* in Proceedings of the 36th Annual Precise Time and Time Interval (PTTI) Systems and Applications Meeting, 7-9 December 2004, Washington DC, USA (U.S. Naval Observatory, Washington, D.C.), pp. 339-354.

[13] D. Strekalov, A. B. Matsko, N. Yu, A. A. Savchenkov, and L. Maleki, 2006, *"Application of vertical cavity surface emitting lasers in self-oscillating atomic clock,"* **Journal of Modern Optics, 53,** 2469-2489.

[14] S. Knappe, V. Gerginov, P. D. D. Schwindt, V. Shah, H. G. Robinson, L. Hollberg, and J. Kitching, 2005, *"Atomic vapor cells for chip-scale atomic clocks with improved long-term frequency stability,"* **Optics Letters, 30,** 2351-2353.

[15] M. V. Balabas, D. Budker, J. Kitching, P. D. D. Schwindt ,and J. E. Stalnaker, 2006, *"Magnetometry with millimeter-scale antirelaxation-coated alkali-metal vapor cells,"* **Journal of the Optical Socety of America B, 23,** pp. 1001-1006.

[16] G. C. Bjorklund, M. D. Levenson, W. Lenth, and C. Ortiz, 1983, *"Frequency modulation (FM) spectroscopy - Theory of lineshapes and signal-to-noise analysis,"* **Applied Physics B, 32,** 145-152.

[17] For example: Accubeat commercial rubidium atomic frequency standard AR-40; Symmetricom 8100 ruggedized rubidium oscillator.

[18] J. Kitching, H. G. Robinson, L. Hollberg, S. Knappe, and R. Wynands, 2001, *"Optical-noise in laser-pimped, all-optical microwave frequency references,"* **Journal of the Optical Society of America B, 18,** 1676-1683.

[19] I. Ben-Aroya and G. Eisenstein, 2005, *"Characterizing absorption spectrum of natural Rubidium by using a directly modulated VCSEL"* in Proceedings of 2005 Joint IEEE International Frequency Control (UFFC) Symposium and the 37th Annual Precise Time and Time Interval (PTTI) Systems and Applications Meeting, 29-31 August 2005, Vancouver, Canada (IEEE 05CH37664C), pp. 602-607.

[20] D. V. Kuksenkov, H. Temkin, and S. Swirhun, 1995, *"Polarization instability and relative intensity noise in vertical-cavity surface-emitting lasers,"* **Applied Physics Letters, 67,** 2141-2143.

[21] J. C. Camparo and J. G. Coffer, 1999, *"Conversion of laser phase noise to amplitude noise in a resonance atomic vapor: The role of laser linewidth,"* **Physical Review, A59,** 728-735.

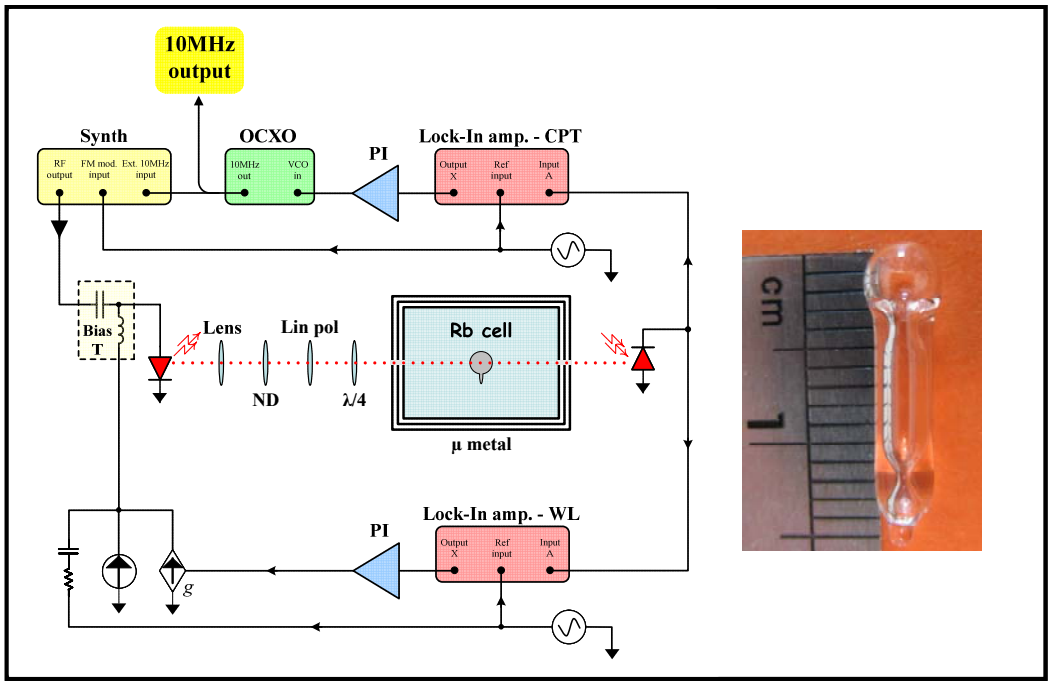

Figure 1. CPT-based clock schematic and a photograph of the Rb cells (insert).

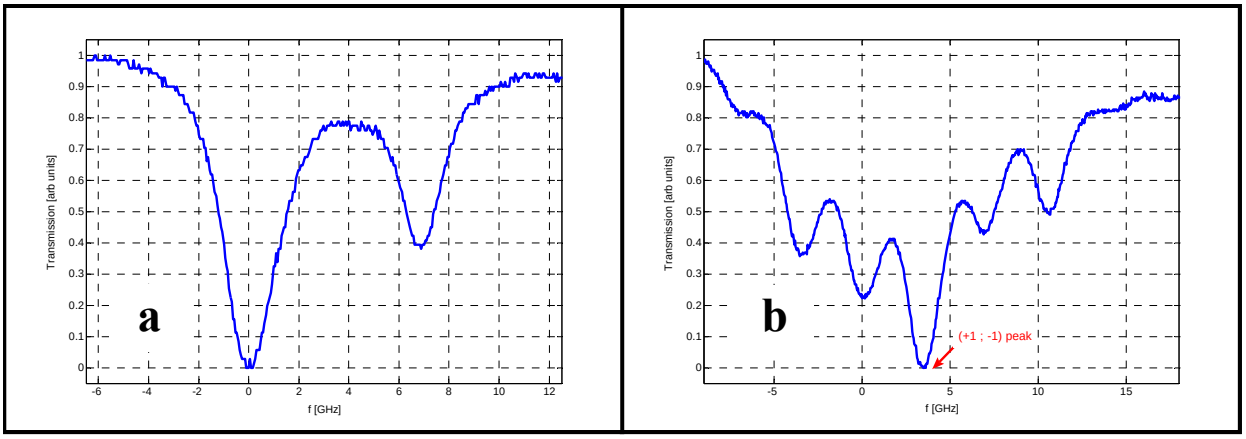

Figure 2. Measured absorption spectra of the small vapor cell: (a) Transmission versus DC bias; (b) Transmission vs. DC bias in the presence of a constant amplitude and constant frequency RF signal. The modulation signal is approximately 3.4173 GHz. The red arrow marks the (+1;-1) peak which is used for the CPT process excitation.

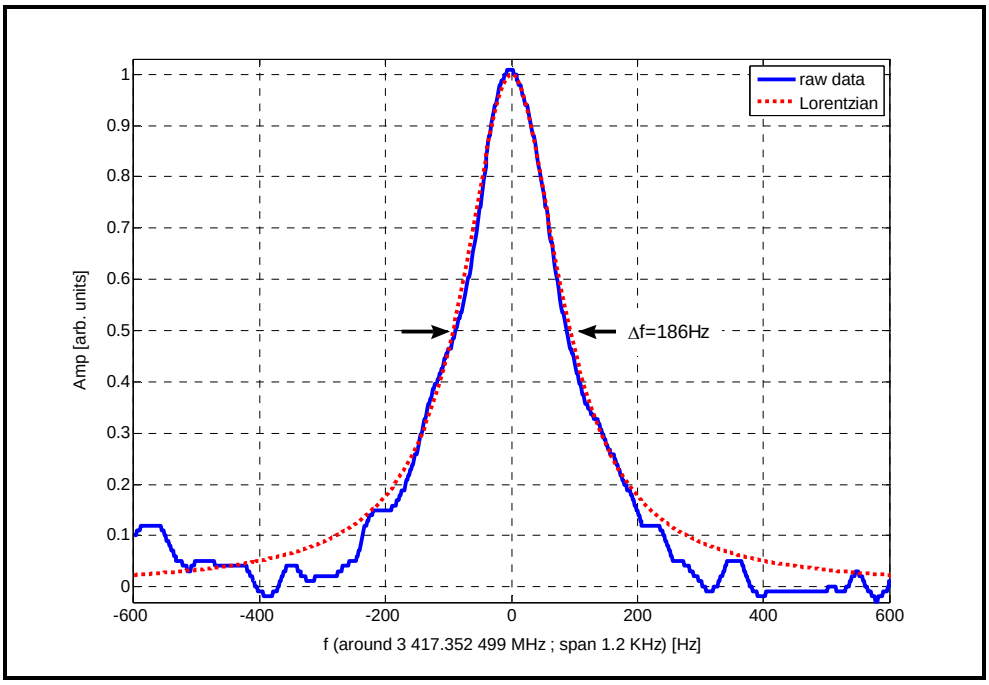

Figure 3. Measured CPT resonance (blue line). The resonance fits a Lorentzian function with a width of 186 Hz (red dashed line).

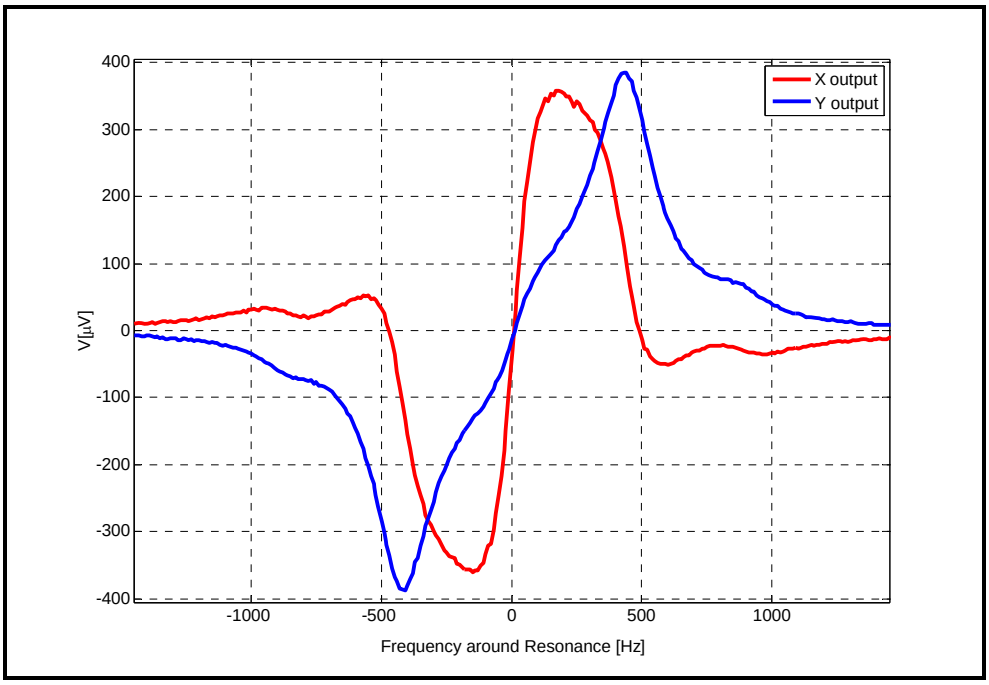

Figure 4. CPT resonance measurement using the FM spectroscopy method. The red curve (x output) is mainly attributed to the 2nd derivative of the dispersion, while the blue curve (y output) is related to the 1st derivative of the absorption.

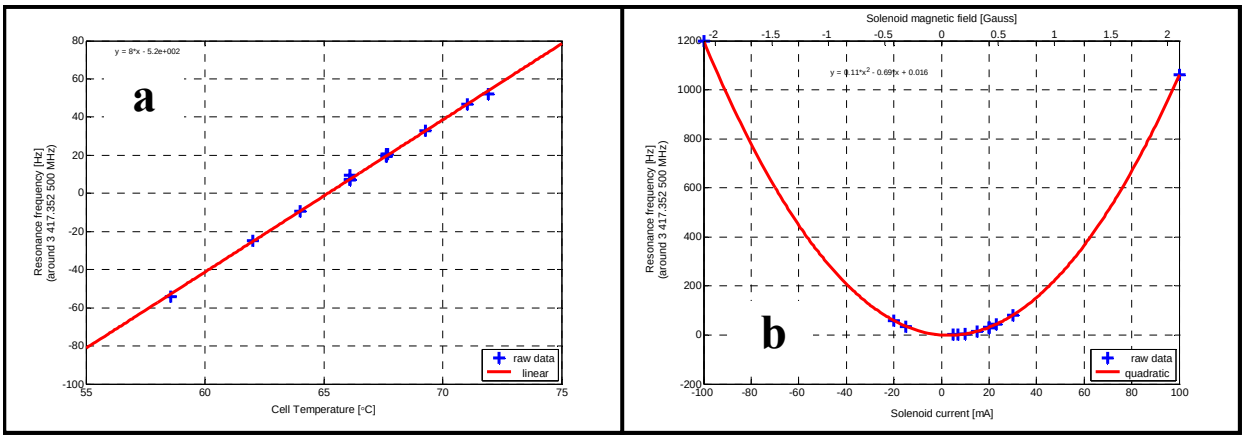

Figure 5. The influences of controlled environmental parameters on the resonance frequency: (a) Measured shift in resonance frequency versus cell operational temperature (blue crosses); the red line represents the linear regression. (b) Measured shift in resonance frequency versus generated magnetic field (blue crosses). The changes are due to the 2nd order Zeeman effect, which accompanies to the 0-0 transition. The red line represents the quadratic regression.

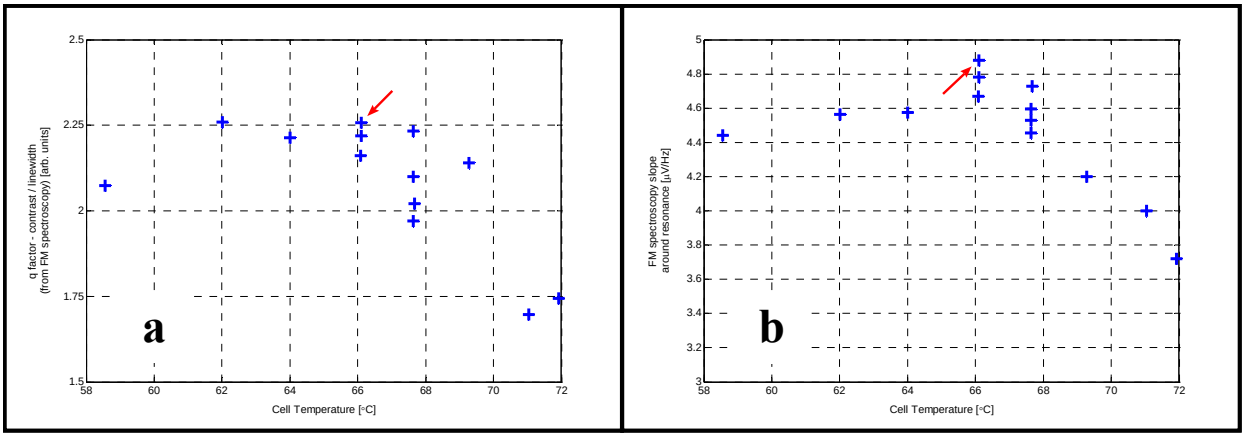

Figure 6. Optimization of the cell operational temperature: (a) Measured q factor versus cell temperature; (b) Measured slope of the FM spectroscopy output signal near the resonance versus cell temperature. The optimum occurs around 66ºC in both graphs and is marked by a red arrow.

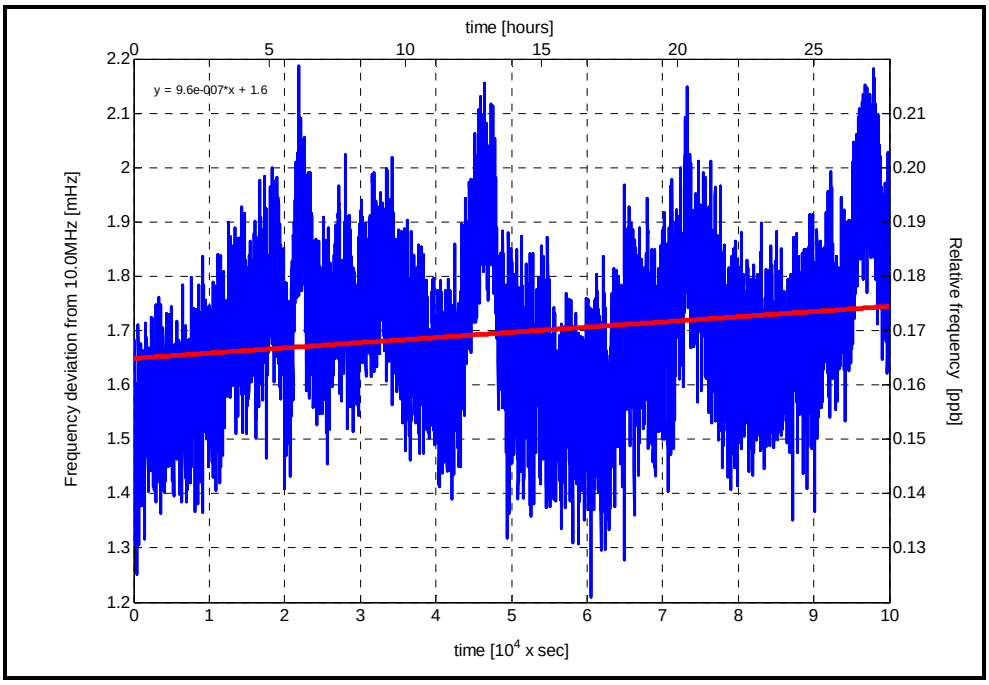

Figure 7. Frequency measurement of the 10 MHz CPT clock output (blue line). The frequency was sampled every few seconds over 100,000 seconds. The red line represents the linear drift in frequency.

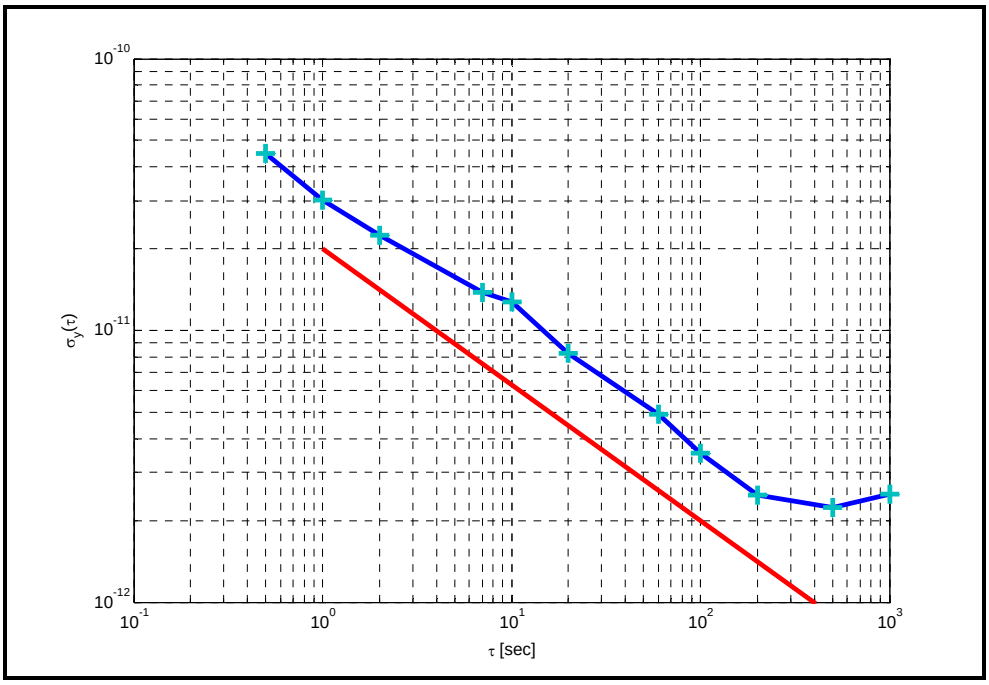

Figure 8. Measured Allan deviation of the clock (blue curve). The red line represents an estimated performance of $2\times10^{-11}/\sqrt{\tau}$.